CrossMark

Acetone sensors based on microsheet-assembled hierarchical Fe_2O_3 with different Fe^{3+} concentrations

Han Wang[1] · Lei Yan[1] · Shuo Li[1] · Yu Li[1] · Li Liu[1] · Liting Du[1] · Haojie Duan[1] · Yali Cheng[1]

Abstract

Several different morphologies of microsheet-assembled Fe_2O_3 have been fabricated by hydrothermal method using diverse concentrations of Fe^{3+} precursor solutions (0.025, 0.020, 0.015, 0.010 mol/L Fe^{3+}). The as-synthesized materials have been characterized by scanning electron microscope (SEM), X-ray powder diffraction (XRD), and energy-dispersive X-ray spectrometry (EDS). The SEM images reflect that the morphologies of as-synthesized materials are affected by the concentrations of Fe^{3+} in precursor solutions. The less concentration of Fe^{3+}, the more porous of Fe_2O_3 microflowers, and thinner of slices distributed on the surface. Furthermore, gas sensors based on these Fe_2O_3 microflowers manufactured and tested to various common gases. The optimum response value to 100 ppm acetone is 52 at the working temperature of 220 °C. Meanwhile, the Fe_2O_3 microflower sensors possess ultrafast response-recovery speed, which are 8 and 19 s, respectively. The possible sensing mechanism was mainly attributed to the high surface area, three-dimensional porous structure.

1 Introduction

A wide range of interest has been generated during the past decades in the field of designing and preparing nanoscale and microscale materials. Especially, three-dimensional (3D) materials have drawn widespread attention since their porous structure is useful to improve the gas sensing characteristics of materials [1–3]. Porous 3D materials possess looser structures and larger surface areas, which is beneficial to the diffusion of gas molecules in the materials and provides more effective areas of attachment. Therefore, porous materials generally have higher sensitivity and faster response-recovery speed [4, 5]. Recently, Zhang et al. synthesized SnO_2–graphene composites for H_2 sensing [6]; Li et al. fabricated ZnO nanosheets for acetone sensing [7].

Among a variety of semiconductor metal oxides, Fe_2O_3 has been widely researched in the field of monitoring toxic gases [8, 9] or detecting flammable gases [10, 11], due to its excellent stable property, low cost, and simple method to facilitate.

Hydrothermal is a widely used method to fabricate nano and micromaterials due to its simple operation and easy control, which can be used to synthesize different morphologies of materials by controlling precursor solution concentrations and experimental temperatures [4, 12].

The previous studies have demonstrated that different morphologies have a great influence on Fe_2O_3 gas-sensing properties, such as Tan et al. synthesis porous α-Fe_2O_3 microrods for ethanol sensing [13], Zhang et al. fabricated V_2O_5-decorated α-Fe_2O_3 nanorods as gas sensor [14] and Cuong et al. synthesized α-Fe_2O_3 nanoparticles for CO gas sensing [15]. However, there are less work research on morphologies influence on gas-sensing properties.

In this paper, we report the fabrication of different morphologies' microsheet-assembled Fe_2O_3 using a simple hydrothermal method combined with a calcination process and gas-sensing performance to acetone gas. By adding different amounts of Fe^{3+} into the precursor solution at the same conditions, four kinds of morphologies of Fe_2O_3 were prepared. Comparing the gas-sensing properties of these four kinds of materials, the test results show that the morphologies of Fe_2O_3 have a big influence on their gas-sensing properties. Among four prepared materials, their optimal working temperature is 220 °C, thin sheet-assembled hierarchical Fe_2O_3 microflowers sensor has a good performance to acetone which is apparently higher than other materials. Therefore, the morphologies of materials have a great

✉ Li Liu
liuli_teacher@163.com

1 College of Physics, State Key Laboratory of Superhard Materials, Jilin University, Changchun 130012, People's Republic of China

influence on their gas-sensing properties, and thin sheet-assembled hierarchical Fe_2O_3 microflowers materials have already possess the value of practical gas-sensing materials.

2 Experimental

2.1 Materials

All chemical reagents were of analytical grade and used without further purification. $FeCl_3 \cdot 6H_2O$ (99.99%), ethanolamine (99%), and ethanediol ($\geq$ 99.0%) were purchased from Aladdin (Shanghai, China).

2.2 Synthesis and characterization of microsheet-assembled hierarchical Fe_2O_3

The experiments were divided into four groups, each group has the same experimental environment except the content of Fe^{3+}. Then, different morphologies microsheet-assembled Fe_2O_3 were synthesized. The experiment process can be described as below. First, a certain amount of $FeCl_3 \cdot 6H_2O$ and 0.34 mL ethanolamine were mixed and dissolved into 60 mL ethanediol to form a transparent solution. After stirring for 30 min, the solution was transferred into a 100 mL Teflon-lined stainless-steel autoclave and kept at 160 °C for 300 min in oven. The obtained products were collected and washed with ethanol several times and dried at 70 °C for 6 h. Finally, the products were calcined in muffle roaster at 500 °C in air for 2 h to obtain Fe_2O_3. In the four groups of experiments, the contents of Fe^{3+} are 0.010, 0.015, 0.020, and 0.025 mol/L, respectively.

The XRD analysis was conducted using a PANalytical Empyrean diffractometer with Cu K_α radiation ($\lambda = 1.5406$ Å). The EDS was performed using a Hitachi S4800 system. SEM images were recorded using a Hitachi S4800 instrument. Transmission electron microscopy (TEM) was recorded on a JEOL-2000F operating at an accelerating voltage of 100 kV. The X-ray photoelectron spectroscopy (XPS) measurements were performed with Al K_α X-ray source. The Brunauer–Emmett–Teller (BET) equation based on the nitrogen adsorption isotherms was used to estimate the specific surface areas of the samples.

The process of gas sensor fabrication can be briefly described as blow. A certain volume of deionized water was mixed with the samples to form a paste. Subsequently, a ceramic tube with a pair of gold electrodes was coated with the paste. A spring-like Ni–Cr wire plugged in the ceramic tube was used to provide the operating temperature. The sensor response ($S = R_a/R_g$) was defined as the ratio of the sensor resistances in the air (R_a) to that in the target gas (R_g). The response time was defined as the time taken by the sensor to achieve 90% of the resistance variation, and the recovery time was the time taken by the sensor to expose to air. The sensing properties of the sensors were measured using a CGS-8 Intelligent gas-sensing analysis system (Beijing Elite Tech Co., Ltd., Beijing, China).

3 Results and discussion

3.1 Morphological and structural characteristics

The XRD patterns provide the crystallinity and phase information of as-prepared Fe_2O_3 powders. As shown in Fig. 1, all the peaks can be readily indexed to the standard diffraction data of Fe_2O_3 (JCPDS No.33-0664). No additional impurity peaks can be detected, which means that all the products were of high purity. Besides, the XRD peaks of four Fe_2O_3 samples with different morphologies are well matched.

The SEM images of microsheet-assembled hierarchical Fe_2O_3 with different Fe^{3+} concentrations are shown in Fig. 2a–d. When the concentration of Fe^{3+} is 0.025 mol/L (Fig. 2a), forming thousands of nanosheets and the morphology of Fe_2O_3 looks like a large sheet with a rough surface and raised particle and the diameter is 5–7 μm and the thickness is 2 μm. When the concentration of Fe^{3+} is 0.020 mol/L (Fig. 2b), forming thick sheet-assembled hierarchical Fe_2O_3 microflowers and microsheets start to crack and expand into thin slices towards different directions; however, the thickness of sheet is large and the number is very small and the diameter is 10–12 μm; the thickness is 2 μm. When the concentration of Fe^{3+} is 0.015 mol/L (Fig. 2c), forming Fe_2O_3 microflowers and the size of Fe_2O_3 sheets becomes into nano level. Numerous
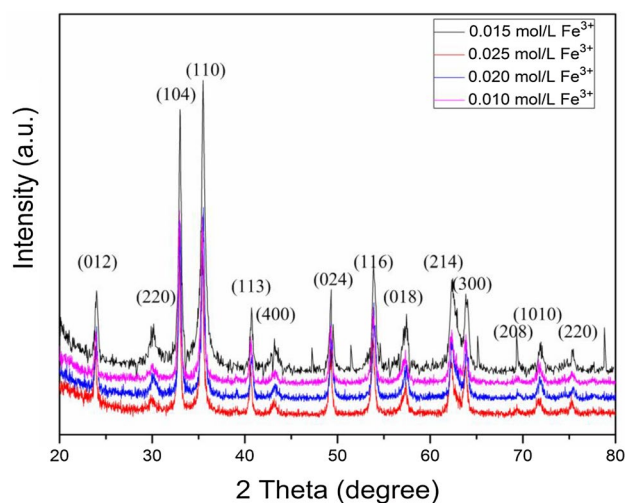
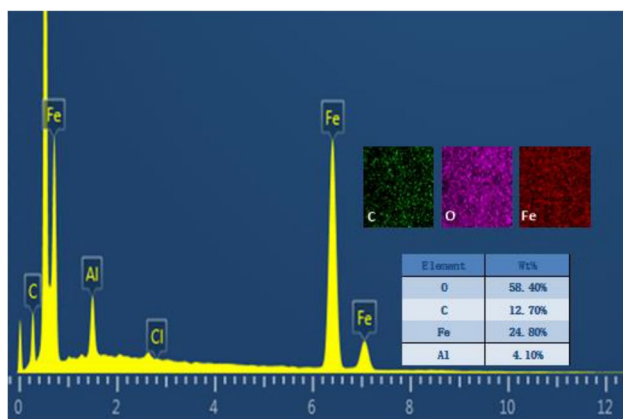**Fig. 1** XRD patterns of microsheet-assembled hierarchical Fe_2O_3 with different Fe^{3+} concentrations
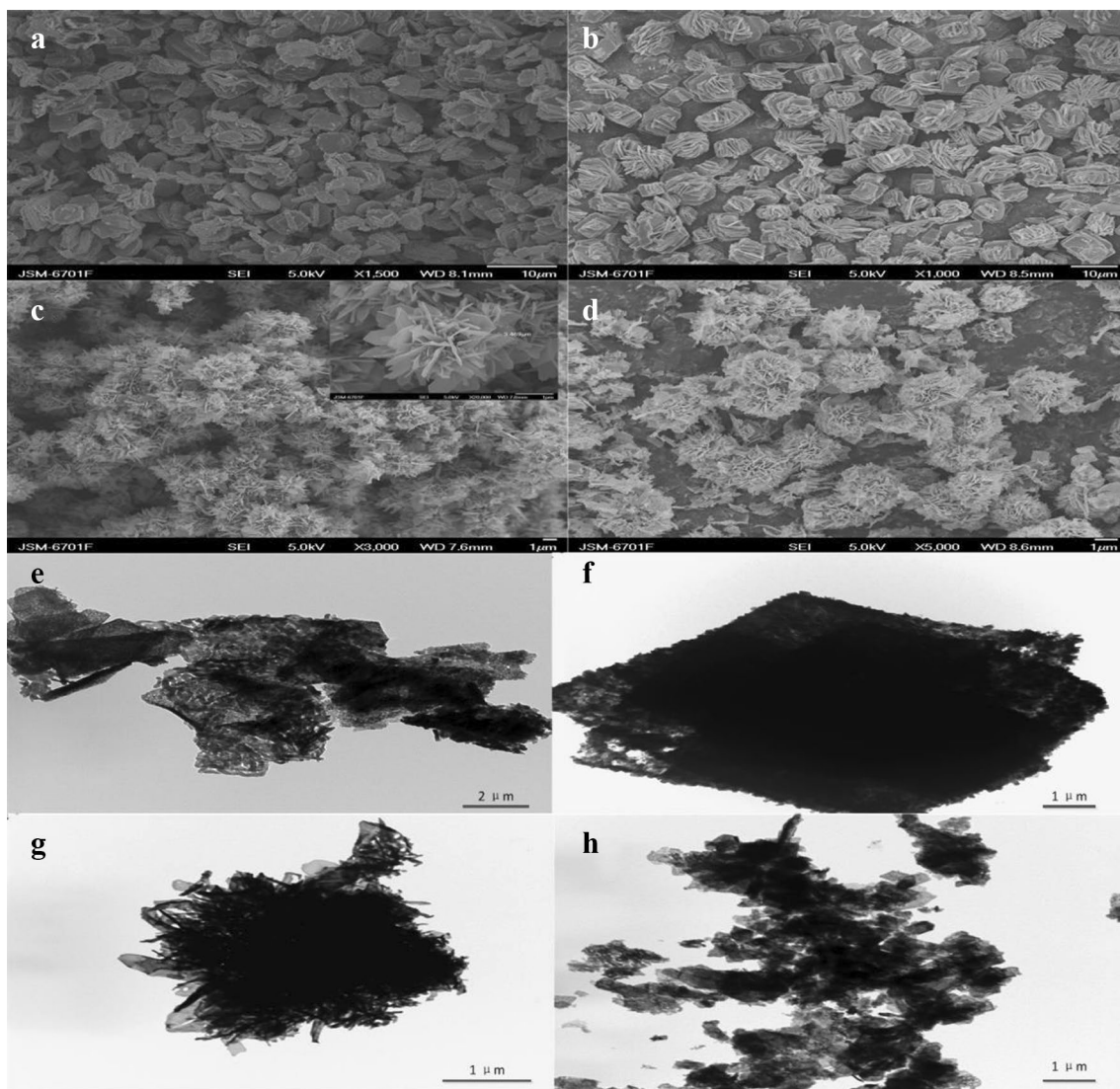
Fig. 2 SEM (**a–d**) and TEM (**e–h**) images of microsheet-assembled hierarchical Fe_2O_3 with different Fe^{3+} concentrations. **a** 0.025 mol/L Fe^{3+}, **b** 0.020 mol/L Fe^{3+}, **c** 0.015 mol/L Fe^{3+}, and **d** 0.010 mol/L Fe^{3+}

randomly arranged flakes are combined into microflowers and the diameter is 3–5 μm; the thickness is below 50 nm, which leading to the extremely loose and porous structure of Fe_2O_3 microflowers. When the concentration of Fe^{3+} is 0.010 mol/L (Fig. 2d), the size of Fe_2O_3 flakes continues to decrease and the diameter is about 5 μm; the thickness is below 100 nm. However, a part of the microflowers begin to break into particles and the uniformity of the material decreases. Combining with the images, as the concentration of Fe^{3+} decreases, the thickness of Fe_2O_3 sheet becomes thinner, and the diameter of the microflower becomes smaller. Figure 2e–h shows the TEM image of Fe_2O_3 microflowers, from which, the solid microflowers with rough surface could be seen clearly. The average grain sizes of these four Fe_2O_3 sample (0.025, 0.020,

0.015, and 0.010 mol/L) is found to be 65, 55, 28, and 35 nm, respectively.

Figure 3 shows the EDS spectra which is collected from microsheet-assembled hierarchical Fe_2O_3 microflowers of 0.015 mol/L Fe^{3+}. Dozens of Fe_2O_3 microflowers are included in the measurement range. This picture demonstrates the existence of Fe and O elements. Besides, there are some other elements existing in the samples, including C, Al, and Cl. The peak of C is derived from the conducting resin during the measurement, the peak of Al is derived from the base carrying test materials, and there is a little of residual Cl element in the sample resulting in the peak of Cl.

The survey spectrum (Fig. 4a) showed the presence of Fe, O, and C elements with peaks corresponding to C 1s, O 1s, and Fe 2p at their characteristic-binding energies [16]. Fe

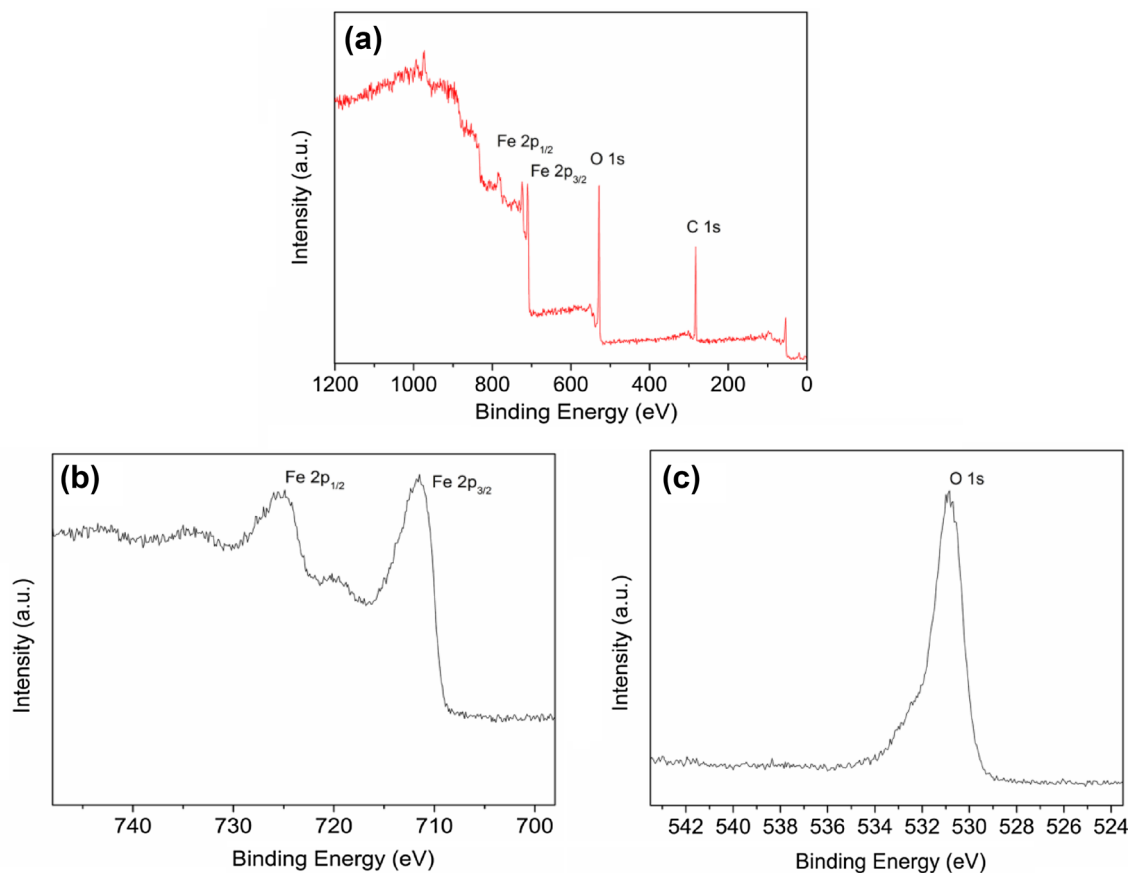**Fig. 3** EDS images of microsheet-assembled hierarchical Fe_2O_3 of 0.015 mol/L Fe^{3+}

2p, O 1s, and C 1s peaks were also studied by their respective high-resolution spectra (Fig. 4b, c). Figure 4b exhibits the main peak of Fe $2p_{3/2}$ appeared at 711.3 eV, along with the Fe $2p_{1/2}$ observed at 725.4 eV, which correspond with the typical values of the ferric (Fe^{3+}) oxides. In Fig. 4c, the binding energy of O 1s was determined to be 530–532 eV,

confirming the oxidation state the composites. The peak of C 1s is derived from the conducting resin during the measurement.

Figure 5 shows the typical N_2 adsorption–desorption isotherms and BJH pore size distribution (inset) of the materials. The Brunauer–Emmett–Teller (BET) surface areas of four kinds of microsheet-assembled hierarchical Fe_2O_3 materials are 23.1, 33.9, 44.1, and 38.5 m^2/g, respectively. In addition, the pore sizes of four kinds of microsheet-assembled hierarchical Fe_2O_3 materials are mainly distributed around 30, 50, 15, and 20 nm, which are displayed in the insets. The BET and BJH results demonstrate that when Fe^{3+} concentrations are 0.015 mol/L it has high specific surface area and proper pore size distribution [6].
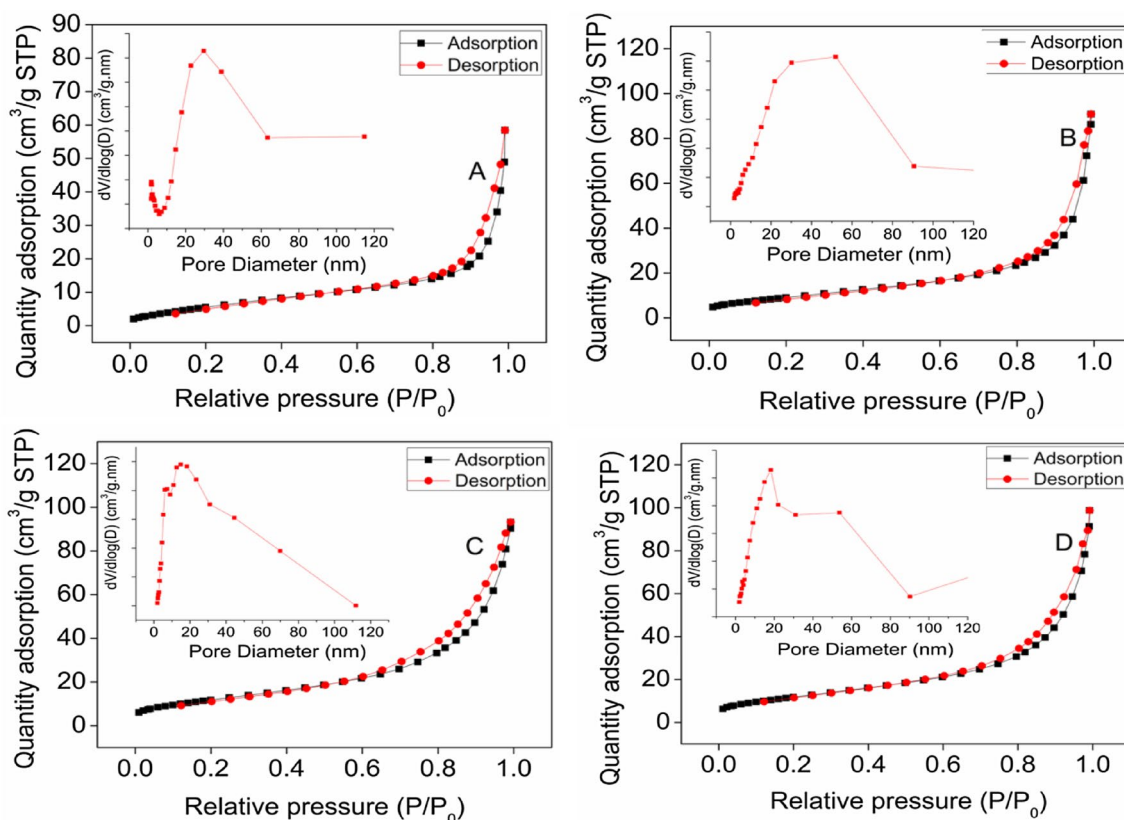
3.2 Gas-sensing properties

The response curves of microsheet-assembled hierarchical Fe_2O_3 with different Fe^{3+} concentrations sensors to 100 ppm of acetone at different operating temperatures are shown in Fig. 6. First, the sensitivity of sensors increases as the temperature increases and reaches the maximum response at 220 °C. This phenomenon can be explained from two
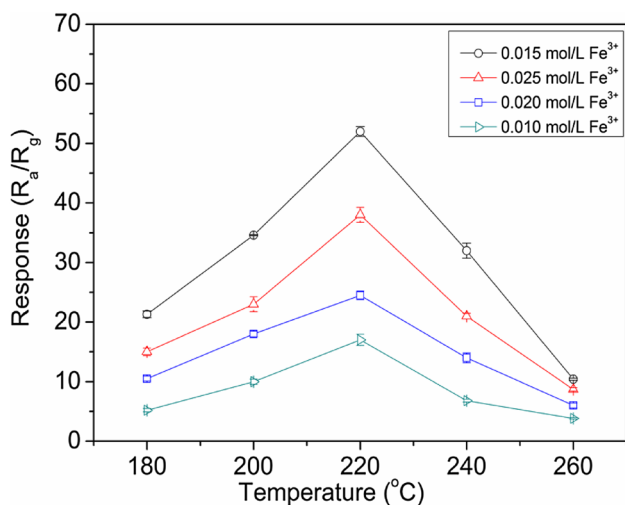

Fig. 4 XPS spectrums of microsheet-assembled hierarchical Fe_2O_3 of 0.015 mol/L Fe^{3+}: **a** survey scan, **b** Fe 2p, and **c** O 1s

Fig. 5 Typical N$_2$ adsorption–desorption isotherms and BJH pore size distribution (inset) of microsheet-assembled hierarchical Fe$_2$O$_3$ with different Fe^{3+} concentrations. **a** 0.025 mol/L Fe^{3+}, **b** 0.020 mol/L Fe^{3+}, **c** 0.015 mol/L Fe^{3+}, and **d** 0.010 mol/L Fe^{3+}

Fig. 6 Responses of microsheet-assembled hierarchical Fe$_2$O$_3$ with different Fe^{3+}concentration sensors towards 100 ppm of acetone versus working temperature
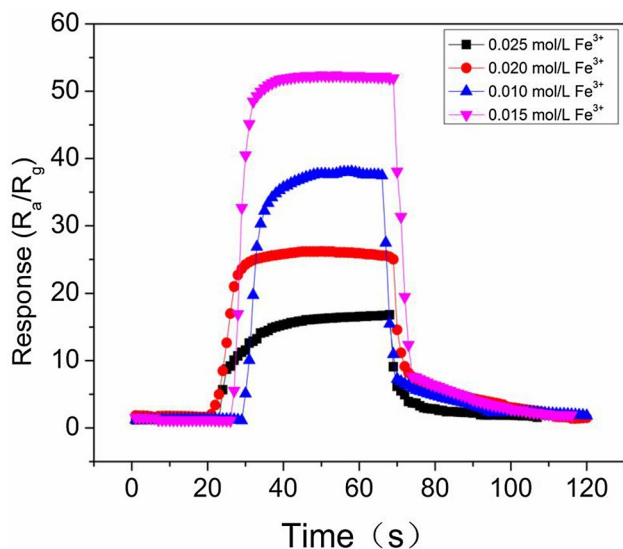
a low temperature, due to the acetone, molecules have not enough thermal energy to react with the surface absorbed oxygen species, and thus, the sensitivity was too low to be detected. The increase in sensitivity for the operating temperatures ranging from 180 to 220 °C can be attributed to the fact that the obtained thermal energy was high enough to overcome the activation energy barrier for the surface reaction. Consequently, the electron concentration increased significantly due to the enhanced surface reaction between acetone molecules and absorbed oxygen species as shown below:

$$CH_3COCH_3 + 8O^- \rightarrow 3CO_2 + 3H_2O + 8e^-.$$
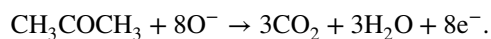
This surface reaction reaches a balance at 220 °C, so the sensitivity of sensors reaches the maximum response at 220 °C. However, when the operating temperature above 220 °C, the sensitivity decreased, which can be attributed to the utilization rate of the sensing layer which was decreased, because the target gas (CH$_3$COCH$_3$) was just consumed at a very shallow surface of the sensing layer in this case, which leads to the reduction of the diffusion depth of the target gas; therefore, the change in the resistance would be decreased. Consequently, the sensitivity decreased [18]. When the

aspects: (1) the kinetic of the reaction between the target gas and surface absorbed oxygen; (2) the kinetic of gas diffusion through the sensing layer [17]. When the sensor operated at
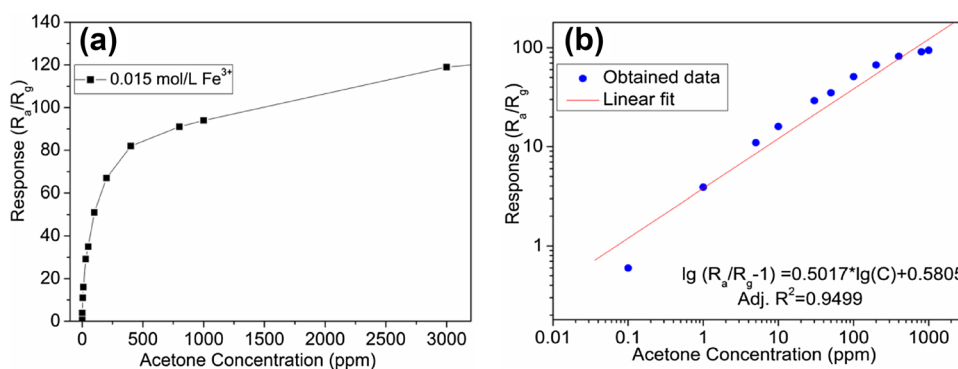
temperature reaches the optimum value, equilibrium adsorption and desorption rate with acetone and oxygen are reached [19], and thus, 220 °C is defined as the optimum temperature of the sensors in subsequent experiments. In addition, among the four sensors based on different samples of different Fe^{3+} concentrations, their responses to 100 ppm acetone at the optimum working temperature of 220 °C EW 17, 26, 52, and 38, respectively. The 0.015 mol/L sample performs better gas-sensing properties compared to other three samples. This behavior depends its high specific surface area and proper pore size distribution, thus leading to the enhancement of gas-sensing properties of the materials.

The response curves of microsheet-assembled hierarchical Fe_2O_3 of different Fe^{3+} concentrations to 100 ppm acetone at 220 °C are presented in Fig. 7. The response and recovery times of 0.015 mol/L Fe^{3+} sample are 8 and 19 s, respectively. Compared with the other 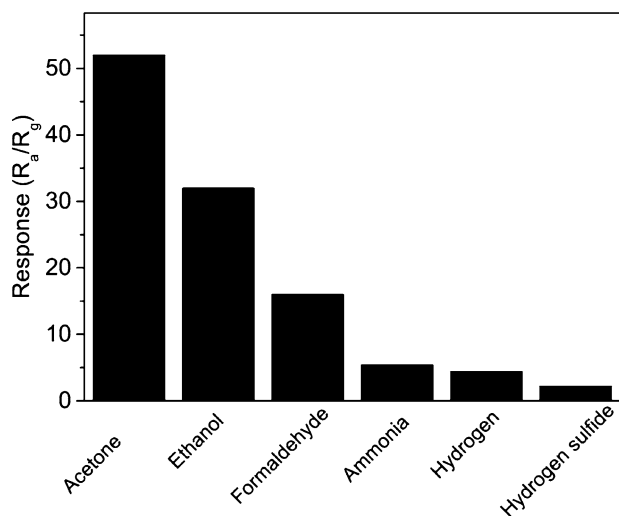three samples, the 0.015 mol/L Fe^{3+} sample still remains a fast response-recovery speed in the case of increased sensitivity. This behavior may be attributed to the unique porous uniform structure of Fe_2O_3. The numerous thin sheets extending around forms an extremely porous and uniform structure, which is favorable for oxygen and acetone gas molecules flow through the entire material and provide more effective attachment points for gas molecules. Meanwhile, acetone gas molecules can easily escape through pores. Therefore, the 0.015 mol/L Fe^{3+} sample can adsorb more gas molecules at constant time, resulting in higher sensitivity and fast response-recovery speed [20, 21].

Figure 8a shows the responses of microsheet-assembled hierarchical Fe_2O_3 microflowers of 0.015 mol/L Fe^{3+} sensor in the range between 0.1 and 10000 ppm of acetone at 220 °C. The sensor response did not reach saturation until 3000 ppm, indicating the large testing scope of acetone. The response (R_a/R_g) of MOS gas sensors is usually empirically represented as $R_a/R_g = a[C]^b + 1$, where a and b are the constants and C is the concentration of the test gas. At a certain operating temperature, the above equation can be rewritten as $\lg(R_a/R_g - 1) = b \lg(C) + \log a$. It can be seen that $\lg(R_a/R_g - 1)$ has a linear relationship with $\lg(C)$: $\lg(R_a/R_g - 1) = 0.5017 * \lg(C) + 0.5805$ (Fig. 8b). The response has a good linear relationship ($R^2 = 0.9499$) with the acetone concentration (0.1–3000 ppm range) in logarithmic forms, suggesting that the microsheet-assembled hierarchical Fe_2O_3 microflowers of 0.015 mol/L Fe^{3+} are excellent sensing materials for the fabrication of practical acetone sensors [22, 23].

Figure 9 shows the sensitivity of microsheet-assembled hierarchical Fe_2O_3 microflowers of 0.015 mol/L Fe^{3+} to 100 ppm of several common gases including acetone, ethanol, formaldehyde, ammonia, hydrogen, and hydrogen sulfide. In practical applications, gas sensor may meet situations of coexistence of multiple gases; in this experiment, the sensor shows less sensitivity to other gases compared to acetone, indicating the good selectivity of the as-synthesized materials.

Repeatability and long-term stability are very important properties of gas sensors. Figure 10 displays three dynamic

Fig. 7 Response-recovery time of 0.025, 0.020, 0.015, and 0.010 mol/L Fe^{3+} concentrations of microsheet-assembled hierarchical Fe_2O_3 exposed to 100 ppm of acetone at 220 °C

Fig. 8 Responses of microsheet-assembled hierarchical Fe_2O_3 microflowers of 0.015 mol/L Fe^{3+} sensor to different concentrations of acetone at 220 °C (**a** 0.1–3000 ppm) and the corresponding $\lg(R_a/R_g - 1) - \lg(C)$ plot (**b**)

Fig. 9 Selectivity of microsheet-assembled hierarchical Fe$_2$O$_3$ microflowers of 0.015 mol/L Fe^{3+} to 100 ppm of different gases at 220 °C
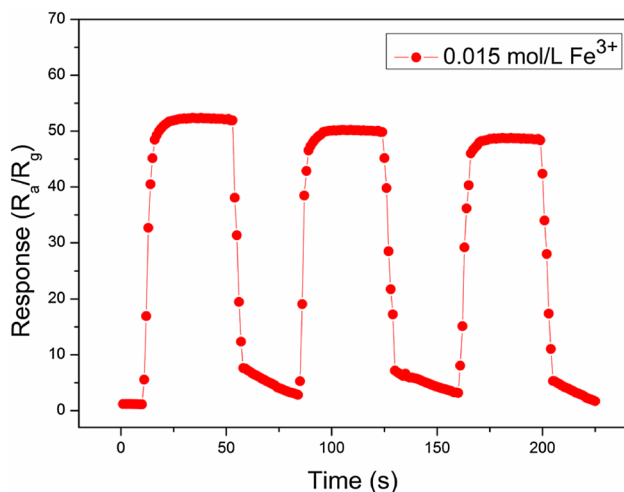

Fig. 10 Three cycles of response-recovery curves of Fe$_2$O$_3$ microflower (0.015 mol/L Fe^{3+}) sensors to 100 ppm of acetone at 220 °C

response and recovery curves of Fe$_2$O$_3$ microflowers to 100 ppm of acetone. The sensitivity value and response-recovery speed almost unchanged during the three cycles, indicating the replicability and stability of the as-prepared materials. Figure 11 shows the sensitivity of Fe$_2$O$_3$ microflower sensors to 20, 50 and 100 ppm acetone within 20 days. It can be seen that the response of gas sensors remained stable generally during the test, demonstrating the long-term stability of Fe$_2$O$_3$ microflowers.

3.3 Gas-sensing mechanisms

The high-gas-sensing performance of the Fe$_2$O$_3$ hierarchical microflowers can be attributed to its porous structure, high

specific surface area, and proper grain size. First, semiconducting metal oxides with porous structures is an important aspect for enhancing gas-sensing performance, which can enable rapid gas diffusion inside the sensing material and enhanced exposed plane [24, 25]. Second, high surface area could be advantageous for gas adsorption/desorption, gas molecular diffusion, as well as for providing numerous active sites for surface-contact reactions to yield enhanced gas-sensing performances [26, 27]. Third, it has been established that the grain size is an important parameter that controls the sensing properties of metal oxide semiconductors. It is generally accepted that sensing materials with a smaller grain size could have a larger sensing response. Meanwhile, the specific surface area of the sensing material could increase with decreasing grain size, leading to enhanced gas adsorption and higher sensitivity [28, 29]. When a sensor is exposed to air, the oxygen molecules will adsorb on the surface of Fe$_2$O$_3$ and consume electrons from the materials, which leading to the increase of material resistance (R_a). The reaction can be described as below [30]:

$$O + e^- \rightarrow O^-$$
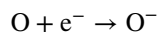
When acetone gas is introduced, the acetone molecules will react with the adsorbed oxygen and release electrons into materials, which leading to the decrease of material resistance (R_g). The reaction can be described as below [31, 32]:

$$CH_3COCH_3 + 8O^- \rightarrow 3CO_2 + 3H_2O + 8e^-.$$
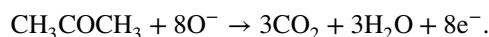
According to the gas sensitivity formula ($S = R_a/R_g$) [33, 34], the more gas the material can adsorb, the greater the difference in resistance creates, which resulting in a higher sensitivity. The porous structure of microsheet-assembled Fe$_2$O$_3$ hierarchical microflowers provides convenient channels and attachment points for gas molecules, so that the diffusion of gas in the materials is easier and more sufficient. Thus potentially enhancing the gas-sensing performance of Fe$_2$O$_3$ materials [32].

The general gas-sensing mechanism of Fe$_2$O$_3$ can be explained as below. When the Fe$_2$O$_3$ microspheres are exposed to air, oxygen will be adsorbed by the Fe$_2$O$_3$ surface and form oxygen species such as O^{2-}, O$^-$, and O^{2-}, which will cause the formation of a depletion region and band bending in the surface region, leading to a decrease in the conductivity of Fe$_2$O$_3$ (Fig. 12a). When a reducing gas such as acetone is adsorbed on the surface of Fe$_2$O$_3$, it will react with the adsorbed oxygen and release electrons into the materials, reducing the depletion region and releasing the band bending (Fig. 12b). Thus, the Fe$_2$O$_3$ conductivity will be improved. In addition, a potential barrier with a height of V$_1$ formed at the Fe$_2$O$_3$–Fe$_2$O$_3$ interface. When the material is exposed to acetone, the acetone

Fig. 11 Long-term stability of Fe_2O_3 microflower (0.015 mol/L Fe^{3+}) sensors
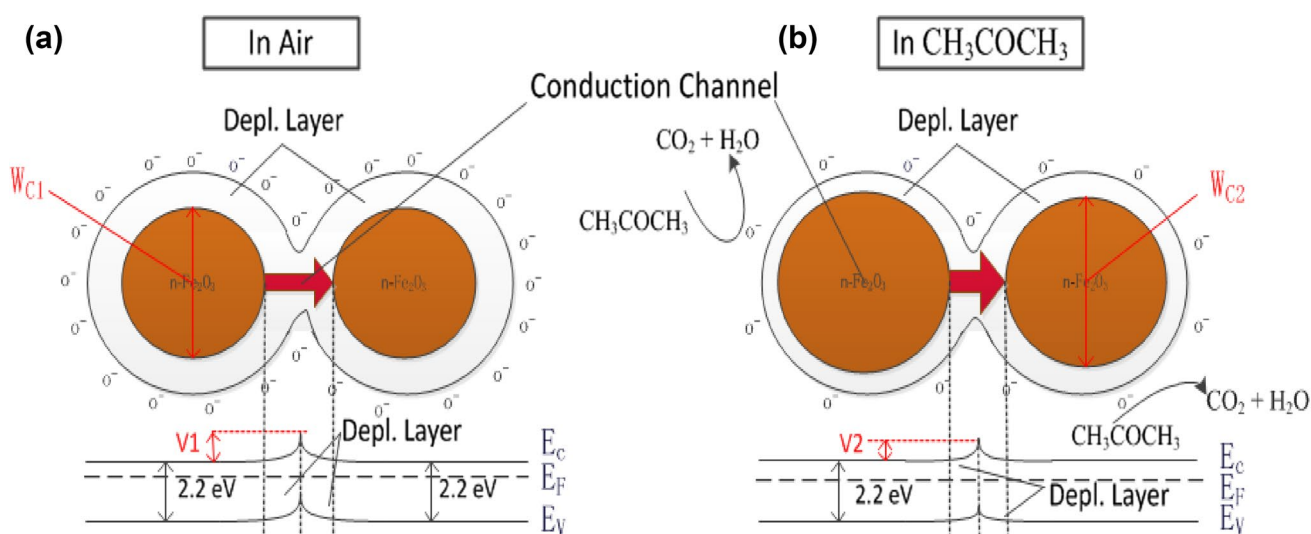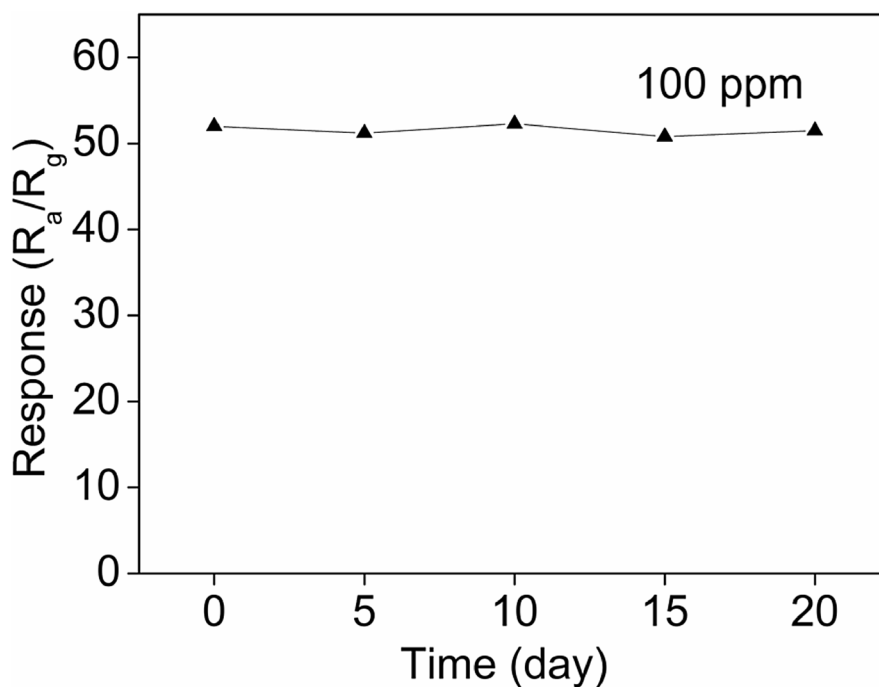
Fig. 12 Schematic illustration of the gas-sensing mechanism of Fe_2O_3 microflower (0.015 mol/L Fe^{3+})

molecules are chemisorbed on the surface of the sensor and react with the adsorbed oxygen species as the formula described above. This reaction leads to an increase in the electron concentration in the surface region of the sensor and a decrease of the resistivity of the sensor. According to the gas sensitivity formula ($S = R_a/R_g$), the gas sensitivity of materials is the result leading by the change of material resistance before and after acetone is introduced [35].

4 Conclusion

In this paper, we synthesized microsheet-assembled Fe_2O_3 using hydrothermal method. Different morphologies of Fe_2O_3 have been prepared by adding different amounts of Fe^{3+} into the precursor solutions. Then, these samples were applied to construct gas sensor devices and their gas-sensing properties were further investigated. When the

concentration of Fe^{3+} is 0.015 mol/L, the sample seems like microflowers and performs the best gas-sensing properties. The SEM images shows that the Fe$_2$O$_3$ are composed of numerous nanosheets. This particular structure makes the microflower extremely porous and the surface area is 44.1 m^2/g, which leading to the improvement of gas-sensing properties. Gas-sensing measurements show the microsheet-assembled hierarchical Fe$_2$O$_3$ microflowers gas sensors have high sensitivity (52 at 100 ppm) and fast response-recovery speed (8/19 s) which is apparently higher than other morphologies' materials. Therefore, when other condition is all the same, materials' morphologies have a great influence to gas sensor's property. Thin sheet-assembled hierarchical Fe$_2$O$_3$ microflower material is suitable as acetone gas sensor material.

References

1. L. Li, C. Zhang, R. Zhang, X. Gao, S. He, M. Liu, X. Li, W. Chen, Sens. Actuat. B Chem. **244**, 664 (2017)
2. A. Dankeaw, G. Poungchan, M. Panapoy, B. Ksapabutr, Sens. Actuat. B Chem. **242**, 202 (2017)
3. Z. Chen, J. Wang, A. Umar, Y. Wang, H. Li, G. Zhou, Appl. Mater. Interfaces. **9**, 11819 (2017)
4. J. Guo, J. Zhang, H. Gong, D. Ju, B. Cao, Sens. Actuat. B Chem. **226**, 266 (2016)
5. K. Shen, Z. Ju, L. Qin, T. Wang, H. Zheng, Dye. Pigm. **136**, 515 (2017)
6. M. Zhang, Y. Zhen, F. Sun, C. Xu, Mater. Sci. Eng. B. **209**, 37 (2016)
7. S. Li, L. Zhang, M. Zhu, G. Ji, L. Zhao, J. Yin, L. Bie, Sens. Actuat. B Chem. **249**, 611 (2017)
8. R. Sonker, B. Yadav, Mater. Today Proc. 3, 2315 (2016)
9. S. Zolghadr, K. Khojier, S. Kimiagar, Mater. Sci. Semicond. Process. **54**, 6 (2016)
10. F. Zhang, H. Yang, X. Xie, L. Li, L. Zhang, J. Yu, H. Zhao, B. Liu, Sens. Actuat. B Chem. **141**, 381 (2009)
11. T. Kim, B. Guo, J. Ind. Eng. Chem. **17**, 158 (2011)
12. L. Liu, P. Song, Q. Wei, X. Zhong, Z. Yang, Q. Wang, Mater. Lett. **201**, 211 (2017)
13. J. Tan, J. Chen, K. Liu, X. Huang, Sens. Actuat. B Chem. **230**, 46 (2016)
14. H. Zhang, Y. Luo, M. Zhuo, T. Yang, J. Liang, M. Zhang, J. Ma, H. Duan, Q. Li, RSC Adv. **6**, 6511 (2016)
15. N. Cuong, D.Q. Khieu, T. Hoa, D. Quang, P. Viet, T. Lam, N. Hoa, N. Hieu, Mater. Res. Bull. **68**, 302 (2015)
16. S.Peshoria1, A. Narula, J. Mater. Sci. **53**, 3876 (2018)
17. L. Li, J. Tan, M. Dun, X. Huang, Sens. Actuat. B Chem. **248**, 85 (2017)
18. Z. Li, Y. Huang, S. Zhang, W. Chen, Z. Kuang, D. Ao, W. Liu, Y. Fu, J. Hazard. Mater. **300**, 167 (2015)
19. C. Liu, X. Wang, F. Xie, L.Liu, J. Mater. Sci. Mater. Electron. **27**, 9870 (2016)
20. X. Wang, J. Zhang, Y. He, L. Wang, L. Liu, H. Wang, X. Guo, H. Lian, Chem. Phys. Lett. **658**, 319 (2016)
21. N. Thu, N. Cuong, L. Nguyen, D. Khieu et al., Sens. Actuat. B Chem. **255**, 3275 (2018)
22. P. Qiao, L. Zhang, M. Zhu, Y. Yin, Z. Zhao, H. Sun, J. Dong, L. Bie, Sens. Actuat. B Chem. **250**, 189 (2017)
23. L. Zhang, J. Zhao, H. Lu, L. Li, J. Zheng, H. Li, Z. Zhu, Sens. Actuat. B Chem. **161**, 209 (2012)
24. J. Jeun, D. Kin, S. Hong, Mater. Lett. **105**, 58 (2013)
25. S. Singh, V. Srivastava, S. Lo, T. Mandal, G. Naresh, Micro. Meso. Mater. **239**, 296 (2017)
26. L. Xiao, S. Xu, G. Yu, S. Liu, Sens. Actuat. B Chem. **255**, 2002 (2018)
27. R. Li, S. Chen, Z. Lou, L. Li, T. Huang, Y. Song, D. Chen, G. Shen, Sens. Actuat. B Chem. **252**, 79 (2017)
28. A. Hastir, N. Kohli, O. Kang, R. singh, J. Eletroceram. **37**, 170 (2016)
29. Q. Zeng, S. Ma, W. Jin, H. Yang, H. Chen, Q. Ge, L. Ma, J. Alloys Compd. **705**, 427 (2017)
30. P. Zhang, H. Qin, W. Lv, H. Zhang, J. Hu, Sens. Actuat. B Chem. **246**, 9 (2017)
31. C. Liu, L. Zhao, B. Wang, P. Sun, Q. Wang, Y. Gao, X. Liang, T. Zhang, G. Lu, J. Coll. Inter. Sci. **495**, 207 (2017)
32. X. Lian, Y. Li, X. Tong, Y. Zou, X. Liu, D. An, Q. Wang, Appl. Surf. Sci. **407**, 447 (2017)
33. J. Cao, Y. Gong, Y. Wang, B. Zhang, H. Zhang, G. Sun, H. Bala, Z. Zhang, Mater. Lett. **198**, 76 (2017)
34. C. Xiang, T. Chen, H. Zhang, Y. Zou, H. Chu, Appl. Surf. Sci. **424**, 39 (2017)
35. I. Sharafeldin, N. Allam, New J. Chem. **41**, 1436 (2017)